4. D.W. Nyby and L.R. Anderson. Finite Element Analysis of Soil-Structure Interaction. In Proceedings of the International Conference on Finite Element Methods (H. Guangqian and Y.K. Cheung, eds.), Science Press, Beijing, China, 1982.
5. G.K. Knight and A.P. Moser. The Structural Response of Fiberglass Reinforced Plastic Pipe under Earth Loadings. Buried Structures Laboratory, Utah State University, Logan, 1983.
6. S. Medrano, A.P. Moser, and O.K. Shupe. Performance of Fiberglass Reinforced Plastic Pipe to Various Soil Loads and Conditions. Buried Structures Laboratory, Utah State University, Logan, 1984.
7. K.D. Sharp, L.R. Anderson, A.P. Moser, and M.J. Warner. Applications of Finite Element Analysis of FRP Pipe Performance. Buried Structures Laboratory, Utah State University, Logan, 1984.
8. J.M. Duncan. Behavior and Design of Long-Span Metal Culverts. Journal of Geotechnical Engineering, ASCE, Vol. 105, No. GT3, March 1979.
9. D.W. Nyby. Finite Element Analysis of Soil-Structure Interaction. Ph.D. dissertation, Utah State University, Logan, 1981.
10. M.G. Katona. Effects of Frictional Slippage of Soil-Structure Interfaces of Buried Culverts. In Transportation Research Record 878, TRB, National Research Council, Washington, D.C., 1982, pp. 8-10.
11. G.A. Leonards, T.H. Wu, and C.H. Juang. Predicting Performance of Buried Conduits. Report FHWA/IN/JHRP-81/3. FHWA, U.S. Department of Transportation, 1982.
12. E.L. Wilson. Finite Element Analysis of Two-Dimensional Structures. Ph.D. dissertation, University of California, Berkeley, 1963.
13. J.M. Duncan, P. Byrne, K.S. Wong, and P. Mabry. Strength, Stress-Strain and Bulk Modulus Parameters for Finite Element Analyses of Stresses and Movements in Soil Masses. Geotechnical Engineering Report UCB/GT/80-01. University of California, Berkeley, 1980.
14. K.D. Sharp, F.W. Kiefer, L.R. Anderson, and E. Jones. Soils Testing Report for Applications of Finite Element Analysis of FRP Pipe Performance: Soils Testing Report. Buried Structures Laboratory, Utah State University, Logan, 1984.

Publication of this paper sponsored by Committee on Subsurface Soil-Structure Interaction.

# The Influence of Interface Friction and Tensile Debonding on Stresses in Buried Cylinders

RUDOLF E. ELLING

ABSTRACT

Underground cylindrical structures, such as pipelines, tunnel liners, and fuel tanks, are subjected to transverse loading that has both static and dynamic origins. The correct evaluation of the stresses and deformation in these cylinders must, in many instances, account for the relative slip between the soil and the cylinder as well as for a partial debonding of the interface surface because of a limited tensile capacity of the soil. Until recently, finite-element methods appeared to offer the only solution technique available with which to handle these difficult interface problems. A study has been conducted of the stresses in buried cylindrical structures with imperfect boundaries through an alternative to the finite-element method that uses assumed stress functions for the soil field as well as for the buried cylinder. The normal stresses and the shear stresses that exist at the soil-cylinder interface are also represented through shape functions. This method has been shown to work efficiently when elastic constitutive laws prevail and under these conditions to be better suited for parametric studies than the finite-element method. The emphasis in this study has been to determine the influence on cylinder stresses of interface boundaries subjected to tensile debonding and tangential slip. Results involving a considerable range of design parameters indicate that tensile debonding does not occur for most cases of practical interest but that tangential slip does occur for most practical designs. Although the interface stress distribution was found to be sensitive to tensile debonding and friction, the tangential hoop stress in the cylinder was found to be surprisingly insensitive to these interface conditions for the cases examined.

Cylindrical structures, such as fuel tanks, pipelines, tunnel liners, and viaducts, are often buried underground and must therefore resist both static and dynamic loading transmitted through the soil. Static loads are imposed as a consequence of the soil's weight and resultant fluid pressure, and from quasi-static loads applied to the surface of the soil; dynamic loads may originate from seismic activity, from underground explosions, or from live loads applied at the surface of the soil. Because buried cylindrical structures are an essential part of the transportation water distribution, waste disposal, and communication systems of most population centers, the correct design of these structures is vital to the welfare of almost everyone.

Because of the vital nature of cylindrical structures to society, considerable attention has recently been focused on the analysis and design of these structures. An excellent overview of the seismic behavior of buried pipelines is given by Wang and O'Roarke (1), and many other research efforts (2-4) have contributed a better understanding of the problems involved in the design of these buried cylinders.

Until recently, almost all analyses of cylinders subjected to transverse loading were based on the assumption of a perfect bond between the buried cylinder and the surrounding soil field. Examples of such analyses have been given previously (5,p.378; 6-8). In some instances, the analysis techniques described in these references permit an assumption of perfect slip, that is, no tangential shear stress at the soil-structure interface. However, these analyses do not incorporate a capacity to deal with an interface surface that is partially debonded because of the limited capacity of a tensile bond between the cylindrical tank and the soil, nor do these analyses include a capability to incorporate arbitrary friction laws at the interface that can reflect the limited capacity of the soilcylinder interface to transfer shear stresses. As a consequence, a significant gap existed in the full understanding of the behavior of buried cylindrical structures until finite-element algorithms were developed that could cope with the problems of an imperfect interface. Among the earliest of the finite-element programs developed to handle slipping interface surfaces were those reported by Chan and Tuba (9) and by Goodman et al. (10). These programs incorporated special finite elements that attempted to simulate the limited capacity of the interface surface to transmit shear and tension stresses. More recently, improved finite-element programs have been developed (11,12) that incorporate interface elements with double nodes; these programs include algorithms that determine whether the double nodes separate in a normal or a tangential direction or remain in full contact based on an evaluation of the state of stress that exists at these nodes.

Although existing finite-element capability now permits a reasonably accurate evaluation of the problems that exist at a not fully bonded interface surface between a cylinder and the surrounding soil, the improved finite-element programs are iterative in nature and comparatively expensive to use. As a result of a research effort sponsored by the National Science Foundation (13), the author has developed an alternative analytical technique that can accommodate tensile debonding and various friction laws at the interface between a cylinder and the surrounding soil when the soil is subjected to transverse loading. This technique, although restricted to cases involving linearly elastic constitutive laws for both the soil and the cylinder, is economical to use and is therefore suitable for parametric studies. The numerical results involving the influence of tensile debonding and interface slip on the resultant stresses in the cylinder, which are reported here, were obtained with this alternative technique.

The analysis technique is limited, theoretically, to deeply buried cylinders, because the soil field is assumed to have boundaries at infinity. However, as has been shown elsewhere (5), results from this type of analysis are valid when the surface of the soil field is beyond only one or two diameters from the buried cylinder.

## MATHEMATICAL FORMULATION OF PROBLEM

A schematic of a representative buried cylinder is shown in Figure 1. The buried cylinder and its surrounding soil field can be modeled as two concentric cylinders, as shown in Figure 2, by considering the free field stresses of the soil field acting on the surface of an imaginary cylindrical boundary in the soil field at a radius much larger than that of a buried tank.

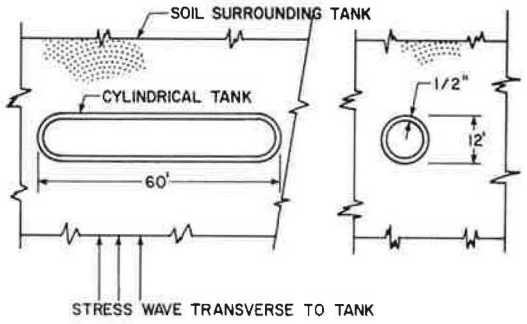


FIGURE 1 Cross sections of representative buried cylindrical tank.

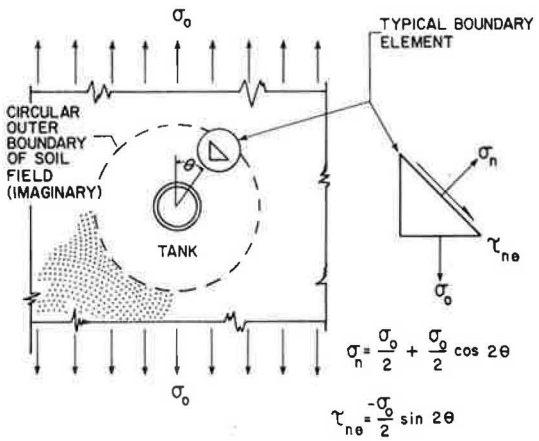


FIGURE 2 Outer boundary of soil considered as circle.

The stresses in the soil field and in the buried cylindrical tank can be expressed through stress functions of the following type (14):

$$\phi = A_0 \log r + C_0 r^2 + (B_1 r^3 + C_1 r^{-1})\cos\theta + \sum_{n=2,3}^{\infty} (A_n r^n + B_n r^{n+2} + C_n r^{-n} + D_n r^{-n+2})\cos n\theta \quad (1)$$

As the author has shown (13), the constants $A_n$, $B_n$, $C_n$, and $D_n$ of the stress function may be evaluated explicitly in terms of the applied free field

stresses in the soil field, the stresses on the inner surface of the buried tank, and the harmonic components of the normal and shear stresses acting at the interface surface between the soil and the tank. When explicit relationships are known for the constants in the stress functions, similar, explicit expressions may also be developed for stresses, strains, and displacements everywhere within the soil field and within the buried cylinder (13).

The normal and shear stresses acting at the interface between the soil and the tank are not known at the outset, but assumptions can be made regarding the region over which these stresses act and the general nature of the distribution of these stresses. As the author has shown (13), for symmetric loading the normal and shear stresses acting at the interface boundary may be expressed in terms of families of functions, as follows:

$$\sigma_r(b,\theta) = \sum_{k=0,1}^{K_1} A_k f^k(\theta,\theta_0) = \sum_{k=0,1,..}^{K_1} A_k [(\cos\theta - \cos\theta_0)/(1-\cos\theta_0)]^k \quad (2)$$

$$\tau_{r\theta}(b,\theta) = \sum_{k=1,2}^{K_2} B_k g^k(\theta,\theta_0) = \sum_{k=1,2,..}^{K_2} B_k \sin[\pi(\theta/\theta_0)^k] \quad (3)$$

where $\theta_0$ is the angle at which tensile debonding begins, as shown schematically in Figure 3. The functions $f^k$ and $g^k$ are chosen so as to permit the normal and the shear stresses to peak at appropriate locations and to reduce values at the location $\theta = \theta_0$ smoothly to zero. The harmonic components of the interface stresses may then be determined in terms of the constants $A_k$ and $B_k$ by Fourier decomposition of the assumed functions $f^k$ and $g^k$.

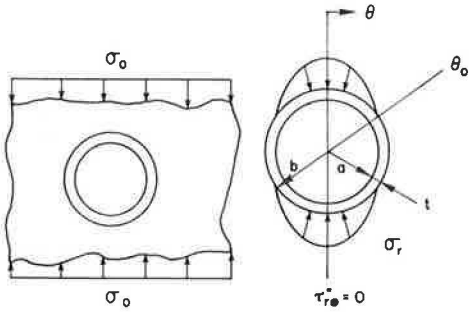


**FIGURE 3 Schematic of partially loaded interface boundary.**

Radial displacements (u), tangential shear stress ($\tau_{r\theta}$), and normal stress ($\sigma_r$) evaluated at the interface surface may then be written for both the soil and the cylinder in terms of the constants $A_k$ and $B_k$. For the general case involving friction and tensile debonding at the interface, equations enforcing radial displacement continuity at the interface are written at specific points (collocation points) along the nondebonded surface of the interface. In addition, equations are also written at specific collocation points along the interface that express the appropriate relationship between the interface shear stress and the corresponding normal stress for a specific friction law. The total number of equations written must equal in number the total number of constants $A_k$ and $B_k$ assumed in the expression for the interface normal and shear stress, respectively. Simultaneous solution of the resulting set of algebraic equations then completes the determination of the unknowns in the problems, because all displacements and stresses are evaluated explicitly in terms of the constants $A_k$ and $B_k$.

If the interface surface is frictionless, only normal displacement continuity need be enforced at the interface. Hence, for these cases the set of algebraic equations that must be solved contains only constants $A_k$ as unknowns. Details of the procedure used to formulate and solve the compatibility equations at the soil-cylinder interface may be found elsewhere (13).

The stress in the soil field is assumed to be uniform with respect to axial location along the cylinder's axis. Therefore, the problem is treated as one of plane strain. For the numerical cases discussed in this report, Poisson's ratio of 0.3 was used for both the soil and the cylinder unless specific differences are indicated.

## TENSILE DEBONDING AT SOIL-CYLINDER INTERFACE

In order to gain a perspective regarding the problem of tensile debonding at the soil-cylinder interface, a study was made to determine the range of design parameters for which such debonding is possible. Specific loadings that were considered in this study involved a uniform compressive stress ($\sigma_y$) of the soil acting in the vertical direction and various values of soil compressive stress ($\sigma_x$) acting in the horizontal direction. The stress $\sigma_y$ may be thought of as an applied stress due to the soil's weight or from a normal load applied to the surface of the soil field, whereas the stress $\sigma_x$ may be considered the result of confining the movement of the soil in the horizontal direction, that is, a Poisson's ratio effect. Thus, if the soil is considered to be completely confined in the horizontal plane, that is, $\varepsilon_x = \varepsilon_z = 0$, the relationship between $\sigma_x$ and the applied soil pressure ($\sigma_y$) is given as follows:

$$\sigma_x = [\nu/(1-\nu)]\,\sigma_y \quad (4)$$

where $\nu$ is the Poisson's ratio of the soil.

For the case of zero friction at the soil-cylinder interface, the region of the cylinder that debonds first is located at $\theta = \pi/2$, where coordinate $\theta$ is shown in Figure 2. A plot of the modulus ratio $E_s/E_t$ versus the ratio of radius to thickness a/t of the cylinder for incipient tensile debonding at $\theta = \pi/2$ is shown in Figure 4 for various ratios of soil stress $\sigma_x/\sigma_y$. Symbols $E_s$ and $E_t$ represent the modulus of elasticity of the soil and the cylinder, respectively. As seen in Figure 4, the relationship between the modulus ratio and the radius/thickness ratio, corresponding to incipient tensile debonding, is essentially linear when plotted on log-log scales. The effect of the confining stress $\sigma_x$ can be seen more clearly in Figure 5, which represents a cross plot of the data shown in Figure 4. As can be seen in Figure 5, tensile debonding does not occur when $\sigma_x > 0.304\sigma_y$. If the soil is completely confined transversely, this limit corresponds to a Poisson's ratio of $\nu = 0.23$.

Another insight into the nature of tensile debonding for a frictionless interface is gained by examining the extent of the region of the interface

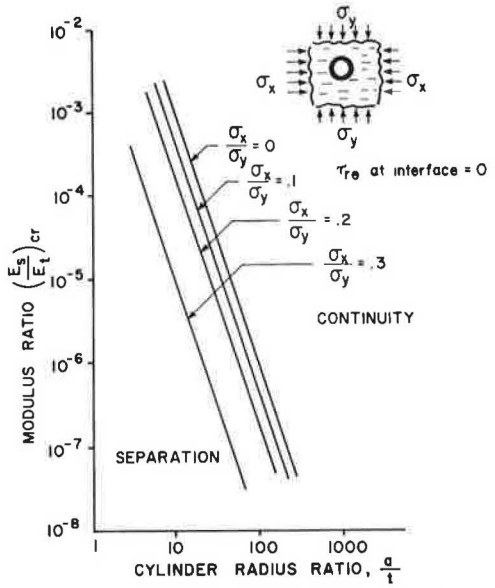


FIGURE 4 Modulus ratio versus a/t required to produce debonding at interface for various ratios of soil stress.

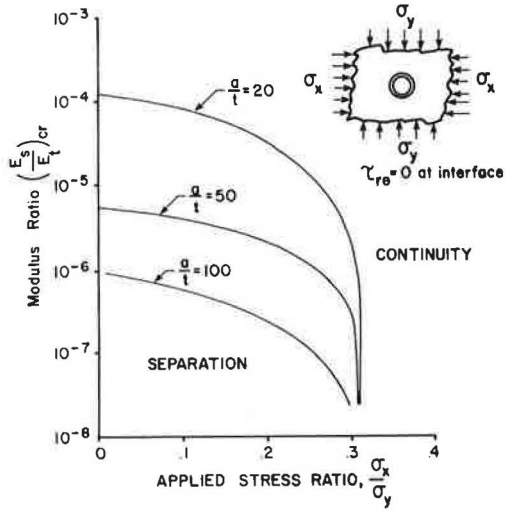


FIGURE 5 Modulus ratio versus applied stress ratio required to produce debonding at interface.

that is subjected to debonding. This is shown in Figure 6 for the case in which the soil is subjected to a uniform compressive stress $\sigma_y = \sigma_0$ and a transverse stress $\sigma_x = 0$. In Figure 6, the angle of separation ($\theta_0$) is plotted as a function of modular ratio $E_s/E_t$. As can be seen from this figure, once separation has been initiated, the angle $\theta_0$ changes rather rapidly as the modular ratio decreases from the value at which separation first started to a value approximately one-tenth of that value. As $E_s/E_t$ is decreased even further, the angle $\theta_0$ changes less rapidly and appears to approach an asymptotic value equal to $\theta_0 = 50$ degrees. The asymptotic value of $\theta_0$ appears to be the same for all values of cylinder radius/thickness ratios examined.

The distribution of normal stress ($\sigma_r$) at the interface for a particular case having tensile debonding is shown in Figure 7. Although it is not obvious from this figure, the peak interface normal stress (evaluated at $\theta = 0$) also appears to approach an asymptotic value ($\sigma_r/\sigma_0 \doteq 2.10$) when the modular ratio is reduced to values even smaller than those shown in Figure 7. The asymptotic value of interface normal stress appears to be the same for all values of cylinder radius/thickness ratios that were investigated.

An insight into the effect of friction on tensile debonding can be gained by assuming a nonslip interface, that is, full tangential displacement continuity at the interface between the soil and the cylinder. A plot of the parameters $E_s/E_t$ versus a/t, corresponding to incipient tensile debonding for this case, is shown in Figure 8 for two values of soil stress ratio $\sigma_x/\sigma_y$. For values of $\sigma_x/\sigma_y > 0.053$, tensile debonding cannot occur for any values of $E_s/E_t$ or a/t. This limiting value of $\sigma_x/\sigma_y$ corresponds to a transversely confined soil field having a Poisson's ratio of $\nu = 0.050$.

Practical values of modulus ratios $E_s/E_t$ are generally $> 10^{-5}$ and radius ratios a/t of pipelines or cylinders used in practice are generally > 5. Therefore, as can be seen from Figures 4, 5, and 7, tensile debonding does not occur for most practical cases of interest when there is even a modest amount of confining soil stress $\sigma_x$ or resistance to tangential slip at the soil-cylinder interface.

The normal stress distribution at a nonslip interface for a particular cylinder design and several modular ratios is shown in Figure 9. The cylinder is assumed to be buried in a soil field having a uniform compressive stress $\sigma_y = \sigma_0$ and $\sigma_x = 0$. Cor-

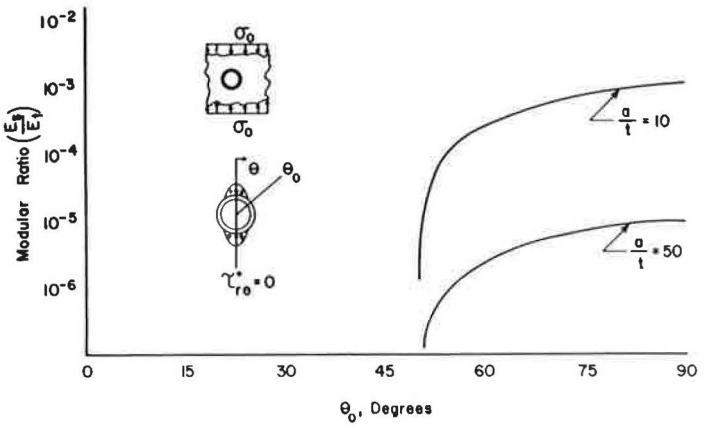


FIGURE 6 Angle of discontinuity $\theta_0$ versus modular ratio.

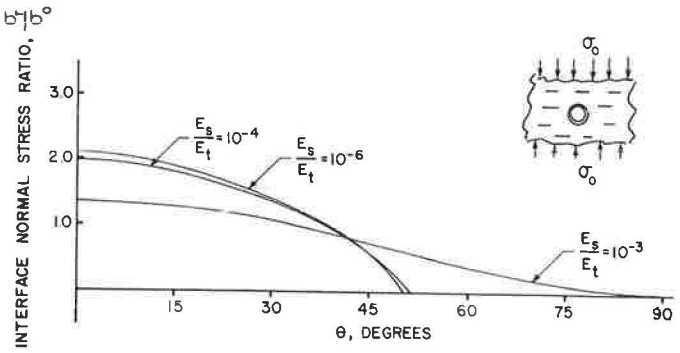


FIGURE 7 Interface normal stress versus $\theta$, a/t = 10, $\tau_{r\theta} = 0$.

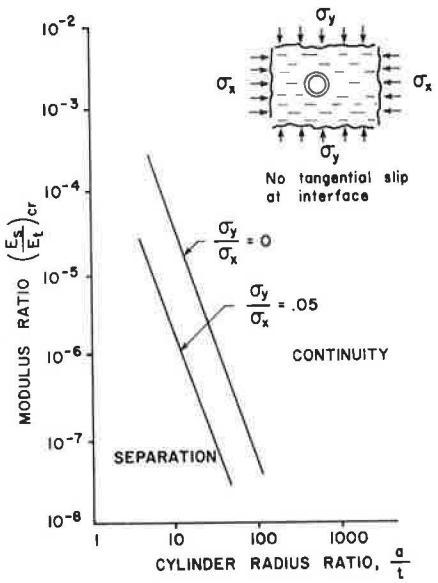


FIGURE 8 Modulus ratio versus a/t required to produce debonding at interface for two values of soil stress.

responding distributions of interface shear stress for these cases are shown in Figure 10. Comparison of values of shear stress shown in Figure 9 with normal stress at corresponding locations of the interface, as shown in Figure 10, indicates that at some regions of the interface the shear stresses are larger than the corresponding values of the compressive normal stress. Therefore, if the tangential bond between the soil and the cylinder is governed by a simple friction law with coefficients of friction less than 1.0, tangential slip is almost certain to occur for the particular cylinder design shown in Figures 9 and 10 as well as for many other practical designs.

Although tensile debonding is not likely for most practical cases of interest when there is resistance to tangential slip at the interface, the influence of friction on the resultant interface normal stress distribution may still be of interest for those cases in which tensile debonding does occur. This is shown in Figure 11 for a moderately thick tank (a/t = 10) buried in a soil field having uniform compressive stress $\sigma_y = \sigma_0$ and $\sigma_x = 0$. The friction law used in this study was a simple Coulomb friction law; thus, the relationship between the shear stress ($\tau_{r\theta}$) and the normal stress ($\sigma_r$) at the interface is expressed as $\tau_{r\theta} = \mu|\sigma_r|$. As can be seen by examining Figure 11, an increasing friction coefficient $\mu$ produces two apparent effects:

1. It reduces the peak normal interface stress $\sigma_r$, and
2. It reduces the region of tensile debonding; that is, it increases the value of $\theta_0$.

As the coefficient of friction increases to values greater than those shown in Figure 11, the resultant normal stress distribution approaches that corresponding to complete displacement continuity at the interface.

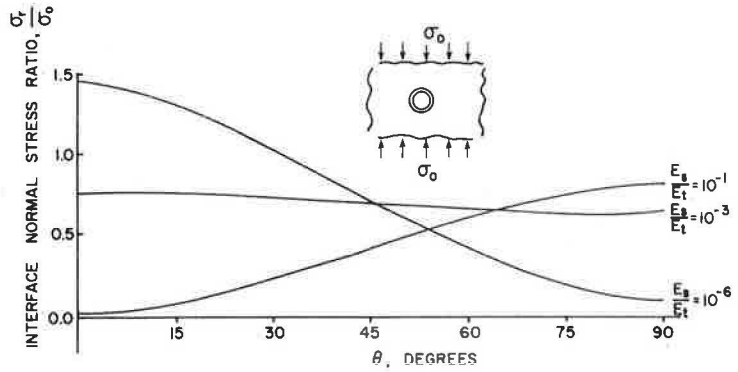


FIGURE 9 Interface normal stress ratio distribution for a/t = 10, $\mu = \infty$.

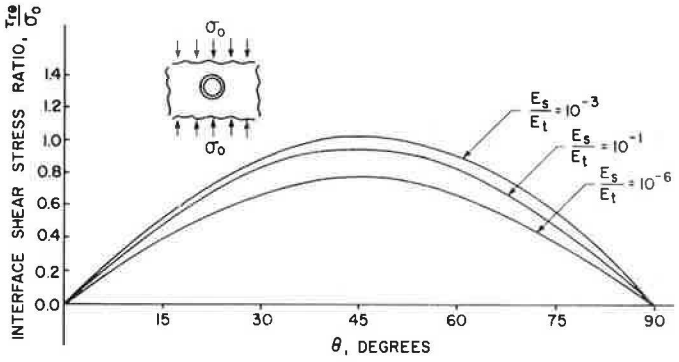


FIGURE 10 Interface shear stress distribution for a/t = 10.

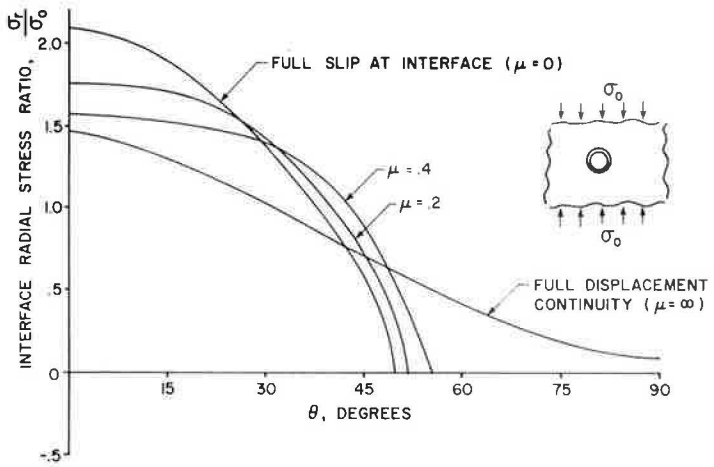


FIGURE 11 Interface radial stress versus $\theta$ for a/t = 10, $E_s/E_t = 10^{-6}$.

## EFFECT OF TENSILE DEBONDING ON CIRCUMFERENTIAL STRESS IN CYLINDER

In the previous section, data were presented indicating that although tensile debonding is unlikely for many practical cases of buried cylinder designs, it may occur for some cases of interest. Therefore, the objective in this section is to explore the effects that tensile debonding and friction have on the resultant circumferential stress in the walls of the cylinder. Results presented correspond to cases having uniform soil compressive stress $\sigma_y = \sigma_0$ and transverse soil stress $\sigma_x = 0$.

Although the circumferential stress in the walls of the cylinder varies in a nonlinear fashion from the inner radius to the outer radius of the tank, the stress may be considered to be a superposition of a uniform stress and a linearly varying flexural stress, such as that shown in Figure 12. The nonlinearity in the radial distribution of the circumferential stress becomes significant only for very thick tanks. The mathematical solution on which the following results are based produces expressions for the more accurate nonlinear distribution of the circumferential stress; the description of the results in terms of a uniform stress and a flexural stress merely aids in interpreting these results.

The maximum circumferential stress in a particular cylinder having a radius/thickness ratio of 10 is plotted as a function of modulus ratio $E_s/E_t$ in Figure 13 for the following cases at the interface:

1. Full displacement continuity,
2. Normal displacement continuity and zero shear stress, and
3. Tensile debonding and zero shear stress.

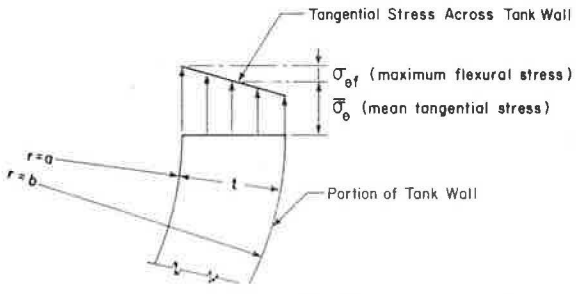


FIGURE 12 Tangential stress distribution across tank wall.

For all cases plotted, the maximum value of circumferential stress approaches an asymptotic value as $E_s/E_t$ is reduced sufficiently; the limiting value for the case with no tensile debonding appears to be approximately 15 percent larger than the limiting value for the case in which tensile debonding is taken into account. In addition, Figure 13 indicates that for all modular ratios, the values of peak circumferential stress ($\sigma_\theta$) are not significantly different when the cases having full displacement continuity at the interface are compared with those having zero shear stress and tensile de-

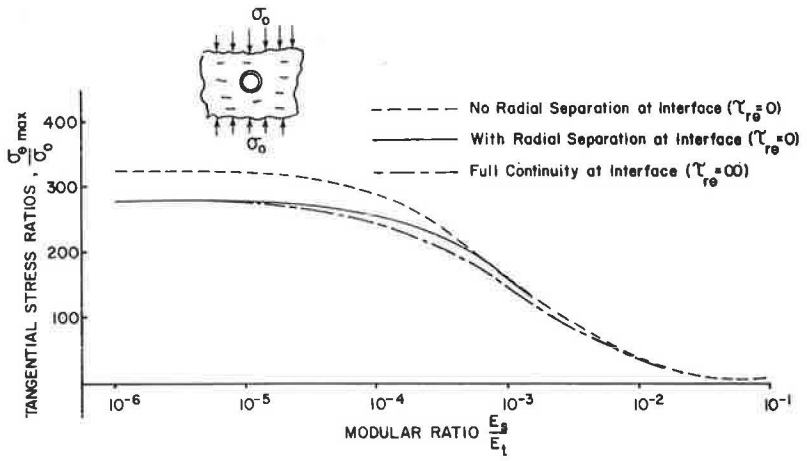


**FIGURE 13** Peak tangential stress ratio $\sigma_{\theta f}$ versus modular ratio for tank with a/t = 10.

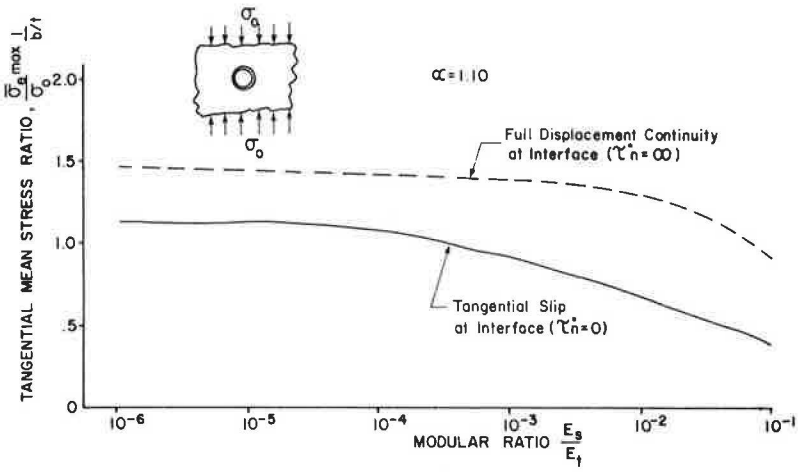


**FIGURE 14** Maximum tangential mean stress ratio versus modular ratio for tank with a/t = 10.

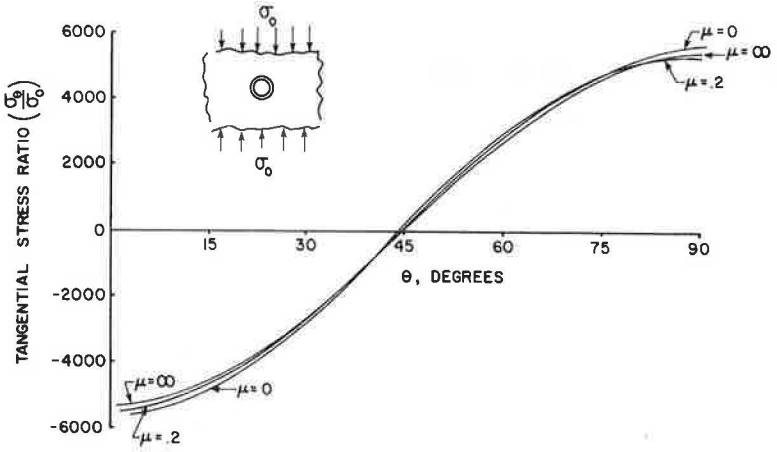


**FIGURE 15** Tangential stress ratio versus $\theta$ for tank with a/t = 50, $E_s/E_t = 10^{-6}$, and several values of $\mu$.

bonding at the interface. Similar results obtained for thinner tanks exhibit the same trends as those shown in Figure 13, although the magnitude of the peak circumferential stress becomes larger as the tank becomes thinner.

The maximum value of circumferential stresses in the walls of the cylinder for those cases plotted in Figure 13 consists primarily of flexural components. A plot of the corresponding peak uniform, or mean, circumferential stress is shown as a function of modular ratio in Figure 14. As can be seen from Figure 14, the value of the mean circumferential stress for the case with tensile debonding and zero interface shear stress is significantly less than the corresponding stress for the case having full interface displacement continuity. However, when the magnitudes of the mean stress plotted in Figure 14 are compared with the maximum circumferential stress plotted in Figure 13, it is readily apparent that the mean circumferential stress is only a small percentage of the total circumferential stress for the particular cases plotted.

Because the values of the peak circumferential stress corresponding to the cases for full continuity at the interface and zero tangential stress with tensile debonding at the interface are nearly the same (as shown in Figure 13), it might be anticipated that the influence of friction on the value of peak circumferential stress in the cylinder walls is a minor one. Results obtained in this investigation verify that the conclusion is a correct one. As an example, the distribution of circumferential stress at the inner walls of the cylinder is shown plotted around the periphery of the cylinder in Figure 15 for a particular set of soil and cylinder parameters. Similar results have been obtained for other sets of soil and cylinder parameters, but they are not plotted here. The remarkable lack of sensitivity of the peak circumferential stress to values of the coefficient of friction and to tensile debonding has been one of the major surprises of this investigation.

## SUMMARY, COMPARISONS, AND CONCLUSIONS

A mathematical technique has been described that is capable of determining the state of stress in both a soil field and a circular cylinder buried in the stressed soil field. The interface between the soil and the buried cylinder may be fully continuous or may be subjected to tensile debonding as well as to tangential slip. For cases in which the interface between the soil and the cylinder is fully continuous and the cylinder wall thickness is comparatively small, the results obtained from the use of the technique described in this paper agree closely with similar results obtained from use of a technique described by Burns and Richards (5). For cylinders with relatively large thickness/radius ratios, for example, concrete tanks, results obtained from use of the technique described in this paper depart from similar results obtained by using the Burns and Richards technique (5). The differences in results, when they occur, can be attributable to the fact that the Burns and Richards technique treats all cylinders with thin-shell theory, whereas the technique described in this paper treats the cylinder with a consistent stress function formulation that is valid, within the bounds of the theory of elasticity, for all cylinder thicknesses.

This study has focused primarily on determining the influence of a nonperfect interface between the soil and the buried cylinder, that is, an interface subjected to tensile debonding as well as to tangential slip. Tensile debonding at the interface occurs when the normal interface stress exceeds the tensile bonding capacity between the soil and the cylinder, and tangential slip occurs when the interface shear stress exceeds values established by an appropriate friction law. Observations and conclusions determined from this study include the following:

1. Tensile debonding at the soil-cylinder interface is unlikely if the soil field is subjected to biaxial compressive stress but definitely possible if the soil field is subjected to a uniaxial compressive state of stress.
2. Tangential slip at the interface between the soil and the cylinder is likely for many practical cases of interest.
3. For cases involving cylinders buried in a uniaxially compressed soil field, the region of tensile debonding at the interface approaches an asymptotic value as the ratio of the soil modulus to the cylinder modulus decreases to very low values; also, for these cases the maximum interface normal stress approaches an upper limit asymptotically as the modular ratio decreases.
4. The flexural component of the tangential stress in the walls of the cylinder appears to be remarkably insensitive to conditions involving tensile debonding and interface friction; that is, the peak flexural component of the tangential stress in the cylinder walls remains nearly the same whether an idealized, perfect interface or a nonidealized interface is assumed.
5. The mean, or average, value of tangential stress in the walls of the cylinders varies significantly, depending on the assumptions made regarding tensile debonding and friction at the soil-cylinder interface. In general, increasing friction at the interface reduces the region of tensile debonding but increases the peak value of mean tangential stress.

Although the conclusions reached in this study apply to many cases of interest, it should be borne in mind that the mathematical solution is based on the use of linear constitutive laws for both the soil and the cylinder. Hence, the results obtained in this study may no longer be valid when soil strains are sufficiently large so that soil stresses cannot be predicted with reasonable accuracy through the use of a linear stress-strain relationship, a situation that occurs in many practical cases. In addition, many practical loading conditions involving buried cylinders produce nonuniform states of stress in the soil field. These cases have not yet been explored and the conclusions stated above may require reexamination when results from such cases become available.

## ACKNOWLEDGMENT

Financial support for this research from the National Science Foundation is gratefully acknowledged.

## REFERENCES

1. L.R. Wang and M.J. O'Roarke. An Overview of Buried Lifeline Earthquake Engineering. Technical Report 1A. Rensselaer Polytechnic Institute, Troy, N.Y., Jan. 1978.
2. N. Hamoda, H. Izumi, and S. Sato. Behavior of Underground Tanks During Earthquakes. Proc., Japan Earthquake Engineering Symposium, Tokyo, 1975.

3. H. Kondo. Response of a Circular Cylindrical Tank to Earthquakes. Presented at Symposium on Lifeline Earthquake Engineering, Portland, Ore., June 1983.
4. K.M. Nova and A. Hindy. Dynamic Response of Buried Pipelines. Proc., 6th European Conference on Earthquake Engineering, Dubrovnik, Yugoslavia, Sept. 1978.
5. J.Q. Burns and R.M. Richards. Attenuation of Stresses for Buried Cylinders. Proc., Symposium on Soil-Structure Interaction, University of Arizona, Tucson, Sept. 1964.
6. R.E. Elling, S.Y. Tuann, and W.S. Tseng. Stresses in Cylinders Embedded in a Stressed Soil Field. Proc., Fourth Canadian Conference on Earthquake Engineering, Vancouver, June 1983.
7. K. Hoeg. Stresses Against Underground Structural Cylinders. Journal of the Soil Mechanics and Foundation Division, ASCE, July 1968.
8. G.N. Savin. Stress Concentration Around Holes (translated by E. Gros). Pergamon Press, London, 1961.
9. S.K. Chan and I.S. Tuba. A Finite Element Method for Contact Problems of Solid Bodies. International Journal of Mechanical Sciences, Vol. 13, 1971.
10. R.E. Goodman, R.C. Taylor, and T. Brekke. A Model for the Mechanics of Jointed Rock. Proc., ASCE, Vol. 92, No. SM3, May 1966.
11. S.K. Arya and G. Hegemier. Finite Element Method for Interface Problems. Proc., ASCE, Vol. 108, No. ST2, Feb. 1982.
12. M.G. Katona. A Simple Contact-Friction Interface Element with Application to Buried Culverts. International Journal of Numerical and Analytical Methods in Geomechanics, Vol. 7, No. 3, 1983.
13. R.E. Elling. Stresses in Buried Cylindrical Tanks. Department of Civil Engineering Report 8S-83. Clemson University, Clemson, S.C., Dec. 1983.
14. S.P. Timoshenko and J.N. Goodier. Theory of Elasticity, 3rd ed. McGraw-Hill Book Company, New York, 1970.

Publication of this paper sponsored by Committee on Subsurface Soil-Structure Interaction.

# Tensile Properties of Chemically Grouted Sand

**CUMARASWAMY VIPULANANDAN and RAYMOND J. KRIZEK**

ABSTRACT

Although the tensile properties (strength, stiffness, failure strain, and mode of failure) of grouted soils are important in many soil-structure interaction problems, little effort has been directed toward identifying and quantifying the mechanisms responsible for the manifested behavior. In this study chemically grouted sand is considered as a two-phase particulate composite, and the tensile properties are examined at both the particulate and the composite levels. Both the adhesive and cohesive properties of the grout are seen to influence the behavior of grouted sand, and an experimental program was conducted to quantify particular relationships for each. These data, together with the porosity of the sand, are employed to formulate two strength models for predicting the tensile behavior of a grouted sand from a knowledge of the properties of the constituents. Comparisons are made between the tensile and compressive properties of grout and grouted sand, and the development of cracks within the specimen is offered as an explanation for the observed nonlinearity in the stress-strain response when either grouted sand or pure grout cured for more than about 2 weeks is tested in compression.

The increasing use of chemical grouting to solve problems involving soil-structure interaction (tunnel support, underpinning, anchors, etc.) has dictated that more efficient design procedures be developed and that a better understanding of grouted sand behavior under different loading conditions be achieved. Although much current design is based on the assumption that the material can resist only compression and shear forces, tensile forces are encountered in many cases. Interest in the tensile properties of stabilized materials has also been stimulated by efforts to provide crack-free liners for waste ponds and cut-offs for dams. In general, many geomaterials have little tensile strength, and